ACS Catalysis

Research Article

pubs.acs.org/acscatalysis

Tandem Site- and Size-Controlled Pd Nanoparticles for the Directed Hydrogenation of Furfural

Scott M. Rogers,[†,‡] C. Richard A. Catlow,[†,‡,§] Carine E. Chan-Thaw,[∥] Arunabhiram Chutia,[†,‡] Nan Jian,[⊥] Richard E. Palmer,[⊥] Michal Perdjon,[†,‡,§] Adam Thetford,[†,‡] Nikolaos Dimitratos,[†,§] Alberto Villa,[*,†,∥] and Peter P. Wells[*,†,‡,#,&]

[†]UK Catalysis Hub, Research Complex at Harwell, Rutherford Appleton Laboratory, Harwell Oxon, Didcot OX11 0FA, U.K.

[‡]Department of Chemistry, University College London, 20 Gordon Street, London WC1H 0AJ, U.K.

[§]Cardiff Catalysis Institute, School of Chemistry, Cardiff University, Cardiff CF10 3AT, U.K.

[∥]Dipartimento di Chimica, Università degli Studi di Milano, via Golgi 19, 20133 Milano, Italy

[⊥]Nanoscale Physics Research Laboratory, School of Physics and Astronomy, University of Birmingham, Edgbaston, Birmingham B15 2TT, U.K.

[#]Diamond Light Source, Harwell Science and Innovation Campus, Chilton, Didcot OX11 0DE, U.K.

[&]School of Chemistry, University of Southampton, Highfield, Southampton SO17 1BJ, U.K.

Supporting Information

ABSTRACT: The conversion of biomass to useful chemical products requires precise catalytic properties to achieve the required activity, selectivity, and durability. Here we show, through optimized colloidal synthesis, the tandem control of Pd size and site availability for the directed hydrogenation of the bioderived intermediate furfural. Adjusting the temperature of colloidal reduction dictates the size of Pd nanoparticles; in some instances ultrasmall clusters of <20 atoms are achieved. However, changing the solvent system affects the PVA–Pd interaction and relative proportion of available surface sites (corners, edges, planes), allowing us to control the selectivity to the valuable hydrogenation products furfuryl alcohol and tetrahydrofurfuryl alcohol. We demonstrate, through combined experimental and computational studies, that Pd nanoparticle planes are more prone to deactivation through the formation of Pd carbide, resulting in the reduced efficacy of furfural binding. This approach to nanoparticle optimization is an important strategy for producing long-lasting, high-performance catalysts for emerging sustainable technologies.

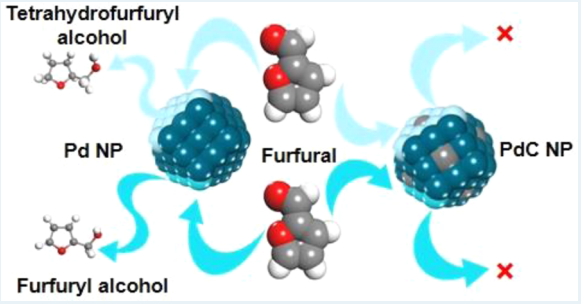

KEYWORDS: *Pd nanoparticles, colloids, clusters, furfural hydrogenation, heterogeneous catalysis, Pd carbide*

INTRODUCTION

Upgrading biomass to useful products, be they energy or platform intermediates, is a crucially important part of a sustainable chemicals industry. The hydrolysis of hemicellulose is one example, where one of the major products, xylose, is acid catalyzed to the valuable intermediate furfural.[1,2] Furfural is readily valorized and is an important precursor in the generation of biofuels[3,4] and chemical intermediates.[2] Furfuryl alcohol, used in the manufacture of resins, adhesives, and synthetic fibers,[5] is produced from the selective hydrogenation of furfural. Subsequent hydrogenation of furfuryl alcohol produces tetrahydrofurfuryl alcohol, a "green solvent", often used in printer inks and agricultural applications.[6] Ultimately, the hydrogenation of furfural results in a complex network of products (Figure 1), where there is a need to control the relative distribution. The challenge is to find a selective catalyst that has control over C=C or C=O hydrogenation and disfavors alternative pathways: e.g., decarbonylation.

Many heterogeneous catalysts have been investigated for the hydrogenation of furfural, with the majority of studies focusing on Cu-, Ni-,[7] Ru-,[8] or Pd-based[9,10] systems. Cu, in the form of Cu chromite[11] or on supports,[12−15] has been commonly used and shows good selectivity to furfuryl alcohol as a consequence of the preference of Cu to bind C=O over C=C.[15] Ni catalysts show different product distributions to Cu, with the primary step favoring decarbonylation and with secondary paths, including opening of the furan ring.[16] Pd is an ideal catalyst for hydrogenation processes, as it readily dissociates hydrogen under ambient conditions. Recent studies have shown that Pd/TiO_2-based systems are effectively able to hydrogenate furfural and furfuryl alcohol under mild conditions (room temperature, 1−3 bar of hydrogen).[17−19] The studies

Received: November 9, 2016
Revised: January 10, 2017
Published: January 17, 2017

DOI: 10.1021/acscatal.6b03190
ACS Catal. 2017, 7, 2266−2274

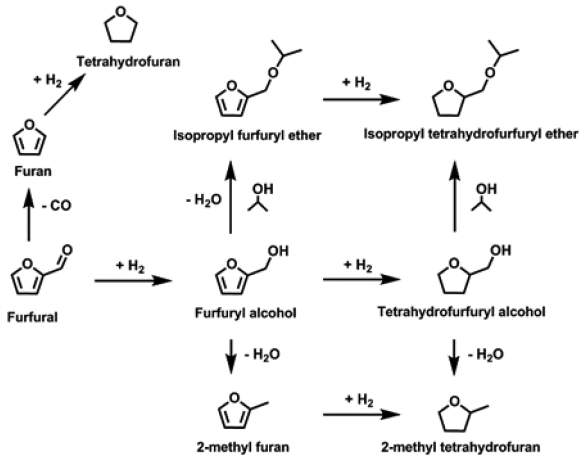

Figure 1. Schematic representation of reaction pathways during furfural hydrogenation.

focused on Pd nanoparticles prepared by incipient wetness impregnation and showed that methylfuran and furfuryl alcohol were the major products and that the product distribution could be altered by changing the solvent of reaction and metal loading.[17] Indeed, the differences in furfural binding (η^1(CO), η^1(O), η^2(C−O), and η^2(C−C)) and their preference for specific crystal facets[20,21] have been linked to variations in product selectivity for different particle sizes.[22] As well as particle size effects, the ability to manipulate the binding orientation of furfural onto specific metal sites, to control selectively the hydrogenation pathway, has been effectively achieved using self-assembled monolayers (SAMs) as blocking agents.[23−25] Medlin et al. used thiolates to block facets selectively, leaving only particle edges/corners exposed.

In this study, we report for the first time how Pd/TiO_2 catalysts prepared through controlled sol-immobilization routes[26] afford series of nanoparticles of tailored particle size distributions, including populations of metal clusters. We show, systematically, how particle size and the solvent system of preparation influences the activity, selectivity, and stability of the catalysts during furfural hydrogenation under mild reaction conditions of 25 and 50 °C. Furthermore, we demonstrate changes to the nanoparticle structure, through carbidization, which causes catalyst deactivation. To our knowledge, this is the first time this deactivation route has been reported.

METHODS

Catalyst Preparation. Supported Pd NPs were prepared using a standard sol-immobilization method with temperature control during the reduction process. K_2PdCl_4 was used to prepare solutions with various H_2O/EtOH ratios of the desired palladium concentration (1.26×10^{-4} M), to which aqueous solutions of PVA (PVA/Pd (w/w) = 0.65) were added. Solutions of $NaBH_4$ (0.1 M; $NaBH_4$/Pd (mol/mol) = 5) were freshly prepared in the respective solvent and added dropwise to each solution over a 1 min period with stirring to form dark brown-black sols. After the complete reduction of Pd species (30 min), the colloidal solution was individually immobilized on TiO_2 (commercial P25) under vigorous stirring conditions. The amount of support material required was calculated so as to give a final metal loading of 1 wt %. The mixture was acidified to pH 1−2 by sulfuric acid before being stirred for 60 min to accomplish full immobilization of the metal NPs onto the support. The slurry was filtered, washed thoroughly with distilled water, and dried overnight at room temperature.

Transmission Electron Microscopy (TEM) and High Angle Annular Dark Field Scanning TEM (HAADF STEM) Imaging. Samples for examination by TEM and aberration-corrected HAADF STEM were prepared by first dispersing the catalyst powder in high-purity ethanol using ultrasonication for 30 min. A 40 μL portion of the suspension was dropped on to a holey-carbon film supported by a 300 mesh copper TEM grid before the solvent was evaporated. A JEOL JEM 2100 EM was used for HAADF STEM analysis at the Nanoscale Physics, Chemistry and Engineering Research Laboratory at the University of Birmingham by using a JEOL JEM2100F STEM equipped with a spherical aberration corrector (CEOS). The HAADF detector was operated with an inner angle of 62 mrad and an outer angle of 164 mrad. An integrated HAADF STEM intensity analysis was used to obtain the size of ultrasmall clusters, with large Pd clusters functioning as mass balances.[27,28] The 3D intensity plot of the small Pd clusters was performed using imagej software.

Infrared CO Chemisorption Studies. Fourier transform infrared (FTIR) transmission spectra were obtained with a Nicolet iS10 spectrometer at a spectral resolution of 2 cm^{-1} and accumulation of up to 64 scans. For each experiment, ∼25 mg of the catalyst was pressed to form a very thin pellet. The cell was purged with helium for 30 min to obtain a background spectrum before CO was introduced using a 10% CO/He mixture at 70 mL min^{-1} over a 30 s period. Three CO doses of this nature were administered for each experiment. The gas was switched to helium for 30 min at 70 mL min^{-1}, in order to remove gaseous and physisorbed CO before obtaining a spectrum.

X-ray Absorption Fine Structure (XAFS). XAFS studies were performed to examine the Pd oxidation state (XANES) as well as the average Pd particle size from the primary shell coordination number (EXAFS). Pd K-edge XAFS studies were carried out on the B18 beamline at the Diamond Light Source, Didcot, U.K. Measurements were performed in transmission mode using a QEXAFS setup with a fast-scanning Si(311) double-crystal monochromator and ion chamber detectors. The time resolution of the spectra was 1 min/spectrum (k_{max} = 18). On average, 15 scans were acquired to improve the signal to noise level of the data. XAS data processing was performed using the Demeter IFEFFIT package.[29,30]

Catalytic Studies. Furfural hydrogenation was performed at 25 or 50 °C, using a stainless steel reactor (30 mL capacity), equipped with heater, mechanical stirrer, gas supply system, and thermometer. Furfural solution (15 mL; 0.3 M in 2-propanol) was placed in the reactor, and the desired amount of catalyst (furfural/metal = 500 mol/mol) was suspended in the solution. The hydrogen pressure was 5 bar. The mixture was left at room temperature (25 °C) or alternatively heated to 50 °C and mechanically stirred (1250 rpm). At the end of the reaction, the autoclave was cooled to room temperature (when performed at 50 °C), the H_2 flow was stopped, and the autoclave was purged with flowing nitrogen. Samples were removed periodically (0.2 mL) and analyzed with an HP 7820A gas chromatograph equipped with an HP-5 capillary column 30 m × 0.32 mm, 0.25 μm film, by Agilent Technologies. Authentic samples were analyzed to determine separation times. Quantitative analyses by an external standard method (*n*-octanol) were carried out.

DFT Studies. The Vienna ab initio simulation package (VASP) was used to perform DFT-based calculations with

DOI: 10.1021/acscatal.6b03190
ACS Catal. 2017, 7, 2266−2274

Grimme's D2 corrections.[31−35] The projector augmented wave (PAW) method was used, and the cutoff energy for the expansion of the plane-wave basis set was set to 550 eV, which gave bulk energies converging to within $10e^{-5}$ eV. A convergence criterion of 0.01 eV/Å for our structural optimizations was adopted. For all the preliminary calculations, the most commonly used Perdew−Burke−Ernzerhof (PBE) version of the generalized gradient approximation (GGA) was used to carry out total energy calculations and perform geometry optimizations.[36] For the bulk calculations, the Brillouin zone was integrated using a Monkhorst−Pack (MP) grid of 11 × 11 × 11 k points. Since it is known that the Pd(111) surface is the most stable surface among the low-index surfaces, all of our calculations were performed on this surface.[37] The ideal Pd(111) surfaces were modeled by a 3 × 3 supercell with 5 atomic layers. A lattice constant of 3.904 Å and a k-point grid of 3 × 3 × 1 was used. During the optimization process, we relaxed the upper two atomic layers along with the furfural molecule. The bottom three atomic layers were fixed to mimic the bulk of the system. The adsorption energy was calculated using the equation

$$E_{ad} = E_{Pd(111)+furfural} - (E_{Pd(111)} + E_{furfural})$$

where E_{ad} is the adsorption energy, $E_{Pd(111)+furfural}$ is the energy of the system with furfural molecule adsorbed, and $E_{furfural}$ is the energy of the furfural molecule.

RESULTS AND DISCUSSION

Characterization of As-Prepared Catalysts. The experimental conditions under which each 1 wt % Pd/TiO_2 catalyst was prepared, as well as notation, is presented in Table 1, with elemental analysis by microwave plasma atomic absorption spectroscopy (MP-AES) shown in Table S1 in the Supporting Information. The prepared Pd/TiO_2 catalysts were characterized using TEM to assess the particle size distribution (Table 1); all images and histograms are detailed in Figure S1 in the Supporting Information.

Table 1. Solvent and Temperature Conditions Applied for Each Pd/TiO_2 Catalyst Preparation, Average Pd Particle Diameter Calculated by TEM Analysis, and XANES Linear Combination Analysis Data for the 1 wt % Pd/TiO_2 Catalysts

				ref standard (%)		
temp/°C	H_2O/EtOH solvent ratio (v/v)	sample notation	TEM av Pd diameter/nm	Pd^{2+}	Pd^0	R_{factor}
1	100	PdA1	2.5 ± 0.8	33	67	0.043
25	100	PdA2	2.7 ± 0.9	29	71	0.037
50	100	PdA3	2.9 ± 1.5*	20	80	0.036
75	100	PdA4	5.2 ± 2.1*	12	88	0.025
−30	50	PdB1	1.4 ± 0.4	71	29	0.056
1	50	PdB2	2.1 ± 0.6	36	64	0.045
25	50	PdB3	3.4 ± 0.9	25	67	0.043

[a]As a consequence of dense agglomeration, only 100 particles were counted.

Within each solvent environment (A series, H_2O; B series, H_2O/EtOH), decreasing the temperature of preparation decreases the average Pd particle diameter, in agreement with our previous work with Au-based materials.[26] PdA1 (2.5 nm) and PdB1 (1.4 nm) produced the smallest Pd nanoparticles within their respective series, with PdB1 exhibiting the narrowest particle size distribution. It is understood that this average particle size is smaller than any previously reported for a Pd/TiO_2 catalyst, synthesized using a PVA/$NaBH_4$ colloidal preparation.[38] The effect of the solvent system can be assessed by comparing samples PdA1 and PdB2 and samples PdA2 and PdB3, which denote samples prepared at 1 and 25 °C, respectively. Interestingly, the B series of Pd/TiO_2 produces a larger spread of Pd particle size as a function of preparation temperature, with catalyst PdB2 being evidently smaller than the A series equivalent (PdA1). However, the distribution of sizes for the A series is much narrower, and the catalyst prepared at 25 °C (PdA2) has a smaller average particle diameter in comparison to the B series analogue (PdB3). We rationalize these differences by the competing influences during sol-immobilization: the rate of metal precursor reduction, solubility of PVA, and interaction of solvent with the metal salt and formed colloid. PdA1 and PdB1 were examined with HAADF STEM to investigate the presence of Pd clusters that are too small to image clearly with standard TEM (Figure 2 and Figure S2 in the Supporting Information). The presence of ultrasmall Pd clusters is clearly evident for catalyst PdA1 and can be identified by the HAADF STEM images. The ability to achieve significant populations of metal clusters through standard chemical means remains a challenge, and in accordance with our previous study,[26] we demonstrate how adjusting the temperature of colloidal reduction is able to influence this.

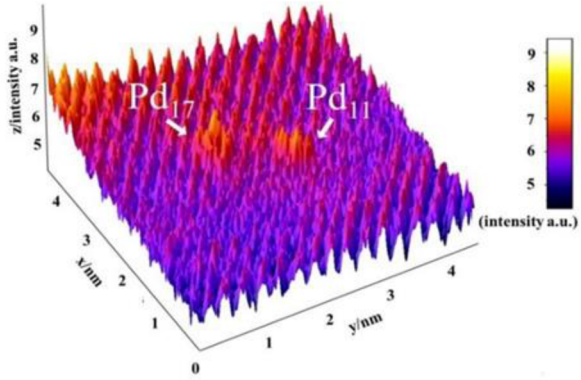

Figure 2. Processed HAADF STEM image of PdA1 showing Pd_{11} and Pd_{17} clusters.

X-ray absorption near edge structure (XANES) is a valuable tool in probing the speciation of metal nanoparticles, in this instance for determining the Pd oxidation state in the Pd/TiO_2 catalysts under atmospheric conditions (during hydrogenation conditions the oxidic content will reduce to Pd metal). The ratio between Pd^{2+} and Pd^0 was performed by linear combination analysis (LCA) of the first derivative of the XANES profile, using PdO and Pd foil as reference standards (Table 1 and Figure S3 in the Supporting Information). It is evident that, for each solvent system, lowering the temperature at which colloidal Pd is prepared results in an increase in Pd^{2+}. All X-ray absorption fine structure (XAFS) measurements represent the whole sample, which means that for NP systems the surface speciation can only influence the overall response for very small NP size; the ratio of surface to core species increases as the average NP diameter decreases. Small Pd NPs form an oxidic surface layer at room temperature on exposure

DOI: 10.1021/acscatal.6b03190
ACS Catal. 2017, 7, 2266−2274

to air,[39] and indeed, we observe a clear correlation between average Pd particle diameter (by TEM) and the extent of Pd^{2+}. The k^2-weighted forward Fourier transform of PdA1 (Figure S3) confirms that there are no large PdO crystallites. The Pd−Pd scattering path that would otherwise be present at 3 Å and can be observed in the PdO reference is not observed in the PdA1 data. With this knowledge, it is understandable that the contribution in the PdB1 catalyst is 71% Pd^{2+} and only 29% Pd^0, due to the very small average Pd size in this catalyst. This information, consistent with TEM analysis, confirms that preparing colloidal Pd NPs at a lower temperature results in a decrease in particle size and the formation of clusters. Pd colloidal preparation at −30 °C in a mixed EtOH/H_2O solvent shows the most significant interest, as the stabilization of ultrasmall metal nanoparticles is challenging but achievable.

To elucidate the specific adsorption sites generated using the different preparation routes, catalysts PdA1, PdA2, PdB1, and PdB2 were evaluated using CO as a probe molecule (Figure 3 and Figure S4 in the Supporting Information). Here, the IR frequency of the CO band was used to assess differences in the surface structure of the Pd NPs. The adsorption band present at 2086 cm^{-1} is assigned to CO linearly adsorbed on corner sites of Pd nanoparticles.[40] There is a secondary linear adsorbed CO band at 2063 cm^{-1}, which can be ascribed to adsorption on Pd nanoparticle edges. Bridge-bonded CO can also be identified at ∼1975 and 1945 cm^{-1}, with the differences in position attributed to adsorption of facets and edges, respectively.[40] Moreover, there are adsorption bands at 2140, 2120, and 1875 cm^{-1}, assigned to CO adsorbed on Pd^{2+}, Pd^+, and 3-fold sites, respectively.[41,42] The spectra obtained for all four catalysts exhibit noticeable differences in the distribution of available sites. The relative intensities of the linearly adsorbed CO bands, in comparison to those from bridge-bonded CO, are much higher for the catalysts prepared in a mixed ethanol−water solvent system. Furthermore, there are differences in the ratio between different types of linear and bridge-bonded sites. The series of NPs prepared in the ethanol−water solvent have a greater proportion of the 2086 cm^{-1} linear adsorbed CO and 1975 cm^{-1} bridge-bonded CO. It is clear that changing the solvent system of preparation affords Pd NPs with different surface characteristics, most notably the increase in available Pd corner and edge sites. We propose that the different surface sites observed are a consequence of the interaction between the solvent and PVA, which affects the extent of PVA binding on the metal surface.

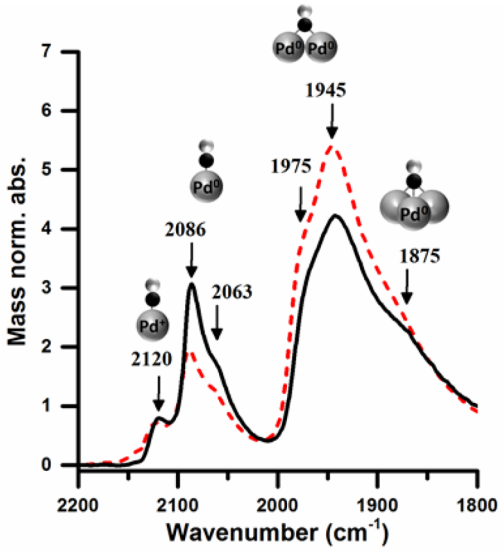

Figure 3. FTIR spectra from CO adsorption studies on PdB1 (solid black line) and PdA1 (red dashed line).

Catalytic Testing. Both series of catalysts were evaluated for the hydrogenation of furfural (furfural 0.3 M; F/metal ratio 500 mol/mol, 5 bar of H_2, solvent 2-propanol) at 25 °C (Table S2 in the Supporting Information) and 50 °C (Table S3 in the Supporting Information), with the data illustrated graphically in Figure 4. On comparison of the data between the A series (prepared in water) and B series (prepared in water−ethanol), interesting relationships can be observed. For the A series there is a clear correlation between Pd particle size and activity; smaller Pd NPs are more active, regardless of the reaction temperature. Indeed, the catalyst of the A series of smallest Pd particle size (A1, 2.5 nm) showed the highest catalytic activity (440 and 620 mol (mol Pd)$^{-1}$ h^{-1}, at 25 and 50 °C, respectively).

For the A series other distinct trends can be seen; as the Pd particle size increases (PdA1 → PdA4), selectivity to furfuryl alcohol increases (48, 65, 76, and 78% for PdA1, PdA2, PdA3, and PdA4, respectively; Table S3 in the Supporting Information) with a decrease in selectivity to tetrahydrofurfuryl alcohol (39, 25, 20, and 15% for PdA1, PdA2, PdA3 and PdA4, respectively; Table S3). On some occasions, the A series catalysts showed improved activity, in comparison to the B series at comparable particle sizes. Catalyst PdA1, with a mean particle size of 2.5 nm, has a higher activity at 50 °C than PdB2 (620 and 470 converted mol (mol Pd)$^{-1}$ h^{-1}, respectively; Table S3), despite the smaller particle size of PdB2 (2.1 nm). It must be noted that these Pd mass normalized activities are high in comparison with current Pd-based catalysts for this reaction.[10,22] There are clearly other parameters, in addition to particle size, that influence activity and selectivity, as can be observed by the catalytic performance of the B series. In the case of the B series tested at 25 °C, the catalyst B1 (1.4 nm) was less active than B2 (2.1 nm) with activities of 491 and 568 mol (mol Pd)$^{-1}$ h^{-1}, respectively. The selectivity of B1 is comparable to that of the only previously reported Pd/TiO_2 catalyst (Pd particle also <2 nm) used for this reaction, despite the different reaction solvent.[17] However, when tests were carried out at 50 °C, there was a direct relationship between particle size and activity. Another characteristic difference of the B series is the variation in selectivity profile with increasing particle size. Broadly speaking, there is an inverse relationship for furfuryl alcohol and tetrahydrofurfuryl alcohol selectivity with particle size in comparison to the A series; as the particle size increases, furfuryl alcohol selectivity decreases and tetrahydrofurfuryl alcohol selectivity increases. It is apparent that there is a collaborative effect between the solvent system and temperature of colloidal preparation, which directs the catalytic performance. It is our assertion that the competing influences of sol immobilization—rate of reduction, PVA solubility, and PVA/solvent/colloid interaction−are responsible for the trends observed. The difference in selectivity can be ascribed to the different binding modes of furfural on the Pd surfaces. The CO chemisorption studies for the A and B series show a clear difference in linear CO to bridged CO ratio, with the B series having a far greater proportion of linear sites. Where CO binds linearly to Pd edge and corner sites, previous studies have indicated that these sites tend to bind furfural in a

DOI: 10.1021/acscatal.6b03190
ACS Catal. 2017, 7, 2266−2274

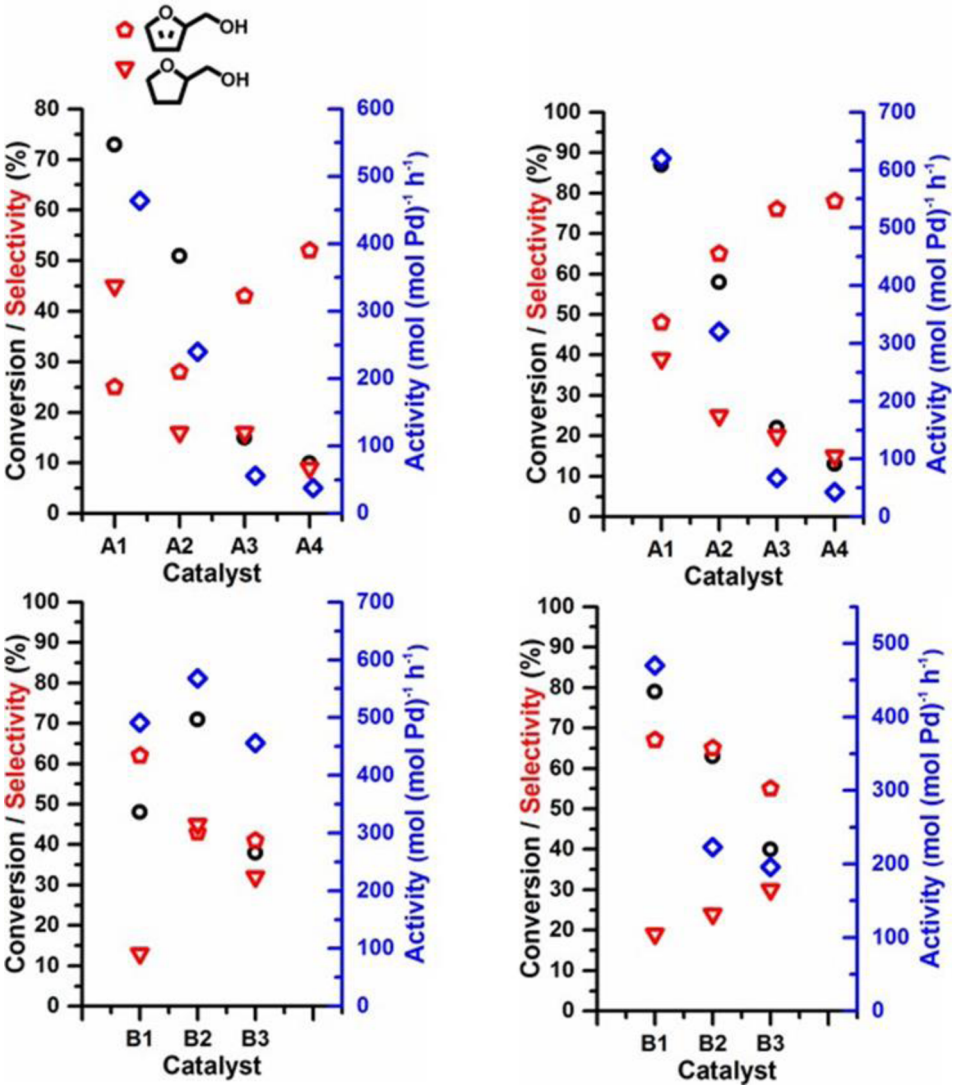

Figure 4. Catalytic performance plots for hydrogenation of furfural using tailored Pd/TiO_2 catalysts: (top left) Pd NPs A1 → A4 tested at 25 °C; (top right) Pd NPs A1 → A4 tested at 50 °C; (bottom left) Pd NPs B1 → B3 tested at 25 °C; (bottom right) Pd NPs B1 → B3 tested at 50 °C. Reaction conditions: furfural 0.3 M; F/metal ratio 500 mol/mol, 5 bar of H_2, solvent 2-propranol. Converted amounts mol (mol Pd)$^{-1}$ h^{-1} were calculated after 15 min of reaction, and the selectivity was calculated at 50% conversion, except catalysts PdA3 and PdA4 at 25 °C, where selectivity was calculated at 10% conversion. Open black circles denote conversion. Open blue diamonds denote activity. Red pentagons and triangles indicate selectivity to the products denoted by the inset key.

perpendicular orientation, rather than flat across a surface, in agreement with the recent work of Medlin et al.[24] In these instances we observe improved selectivity to furfuryl alcohol. Moreover, the adsorption sites that correspond to bridge-bonded or 3-fold CO adsorption are able to bind furfural through both the aldehyde functionality and the furan ring and promote the complete reduction to tetrahydrofurfuryl alcohol. Catalysts used for sustainable technologies need to be robust and durable; therefore, recycling studies were performed. The recycling tests were performed on A1 and B1 catalysts at different temperatures (Tables S4 and S5 in the Supporting Information and Figure 5), by reusing the same catalyst without any pretreatment. These data evidenced a significant deactivation of both catalysts when the reaction was performed at 25 °C, whereas at 50 °C the deactivation was less pronounced. When the reaction profile (Figures S5 and S6 in the Supporting Information) was assessed as a function of time, there is evidence that stronger deactivation phenomena occurred for all of the catalysts when the reaction was performed at 25 °C. To explain the origin of the deactivation, the used catalysts were also characterized.

Used Catalyst Characterization. TEM was used to calculate the average Pd particle size after the recycling experiments were performed at both 25 and 50 °C. The particle size distribution (Figure S7 in the Supporting Information) indicate that, for the samples prepared in water, there is a small increase in average size (2.5 to 2.7 nm for PdA1) when experiments were performed at 25 °C, with no further particle growth when experiments were performed at the higher temperature. However, for the Pd catalysts prepared in an H_2O/EtOH mixture, the temperature of the reaction has a greater influence for PdB1, in which the average particle size increases from 1.4 to 2.0 and 2.7 nm when the reaction was performed at 25 and 50 °C, respectively, and these results are in agreement with the observed initial decrease in catalytic activity. The average Pd particle diameter is still very small, and STEM/

DOI: 10.1021/acscatal.6b03190
ACS Catal. 2017, 7, 2266−2274

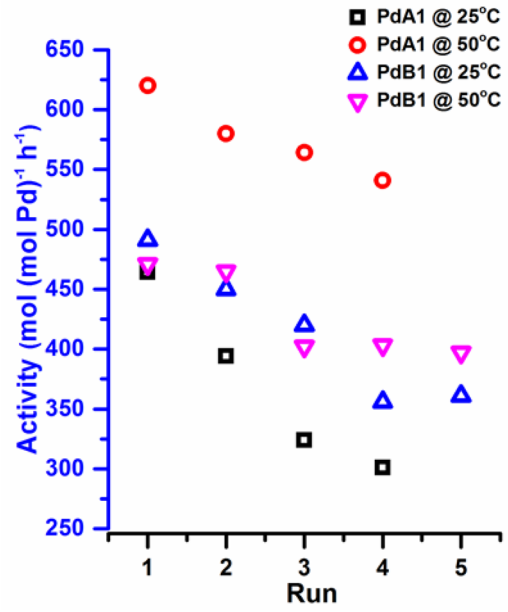

Figure 5. Catalytic activity for recycling studies of catalysts PdA1 and PdB1.

HAADF was used to identify the presence of Pd clusters in the PdA1 and PdB1 catalysts after performing the reaction at 25 °C (Figure S8 in the Supporting Information). It is clear that very small Pd clusters are still preserved during catalysis, which is a combined result of the mild reaction conditions and protective stabilization role of PVA.

The used PdA1 and PdB1 catalysts tested at 25 °C (after five reaction cycles) were assessed using XAFS spectroscopy, with the XANES data shown in Figure 6. The initial observation from the XANES data is the presence of Pd^{2+} and Pd^0. The heights of the main edge of the fresh and used catalysts are greater than that of Pd foil. This difference in height can be attributed to the presence of oxidized Pd in the Pd/TiO_2 catalysts. Elsewhere, the maximum of the second XANES peak

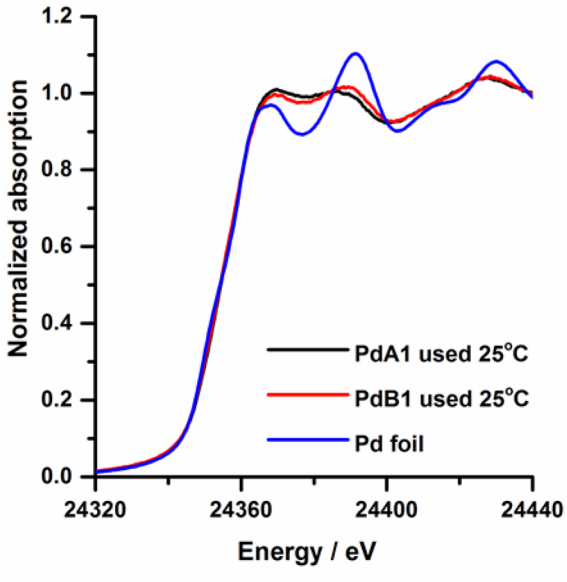

Figure 6. Normalized XANES spectra of PdA1 and PdB1 after catalysis and a Pd^0 reference.

is seen to move to lower energy for the used catalysts, in comparison to the Pd foil. The shift in the position of the second maximum is observed for both hydride and carbide forms of Pd; however, the broadening of the first peak is only observed for carbidic Pd.[43−45] In this instance changes in the first peak maximum are complicated by the separate contribution of oxidized forms of Pd. Further evidence of carbide formation was sought by assessing the EXAFS (Figure 7 and Figure S9 and Table S6 in the Supporting Information), which is able to probe changes in Pd−Pd spacing.

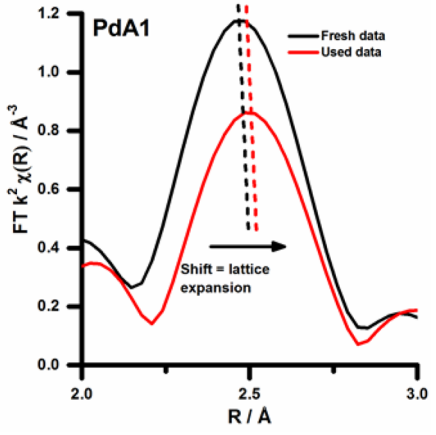

Figure 7. FT χ^2 weighted EXAFS data of fresh (black line) and used (red line) PdA1.

Analysis of the EXAFS data confirms an increase of Pd−Pd spacing after the reaction from ∼2.74 to 2.77 Å. An increase in Pd−Pd spacing is encountered for the formation of Pd carbide and hydride;[39,46] however, hydride is known to readily desorb from the Pd lattice under normal atmospheric conditions. Considering this, it is apparent that this expansion could not be caused by the formation of hydride. The expansion of the Pd lattice from 2.74 to2.79 Å has been previously reported for bulk (PdC_x, where x = 0.13) Pd carbide formation, suggesting that only partial carbidization has occurred.[46] We propose that the deactivation encountered at lower reaction temperature is a result of the transformation to Pd carbide, expansion of the Pd−Pd distance, and the subsequent effect on hydrogen dissociation and the η^2 adsorption of C═O and C═C functionalities. Indeed, a greater degree of deactivation is observed for the catalyst A1Pd (464 → 394 mol (mol Pd)$^{-1}$ h^{-1}) in comparison to B1Pd (491 → 450 mol (mol Pd)$^{-1}$ h^{-1}), which correlates with the extent of carbidization observed. Although we experience deactivation upon carbidization, other catalytic processes experience different effects. Previous work investigating the effect of carbide on the catalytic activity of acetylene hydrogenation concluded that both an increased and decreased activity can be observed, depending on the type of carbidized Pd site (flat, increase; step, decrease).[47,48]

DFT Calculations. To assess the effect of carbidization on the adsorption of furfural, DFT calculations were performed. We first considered two different configurations of furfural, parallel and perpendicular, on a pristine Pd(111) surface (Figure 8a,b). In the case of the perpendicular configuration, we considered the stability of the system on top of a Pd atom (Pd_{top}), on the bridge site between two Pd atoms (Pd_{bridge}), and on the 3-fold hollow site (Pd_{hollow}). The calculated adsorption energy for the parallel configuration ($Pd_{parallel}$) is −2.160 eV,

DOI: 10.1021/acscatal.6b03190
ACS Catal. 2017, 7, 2266−2274

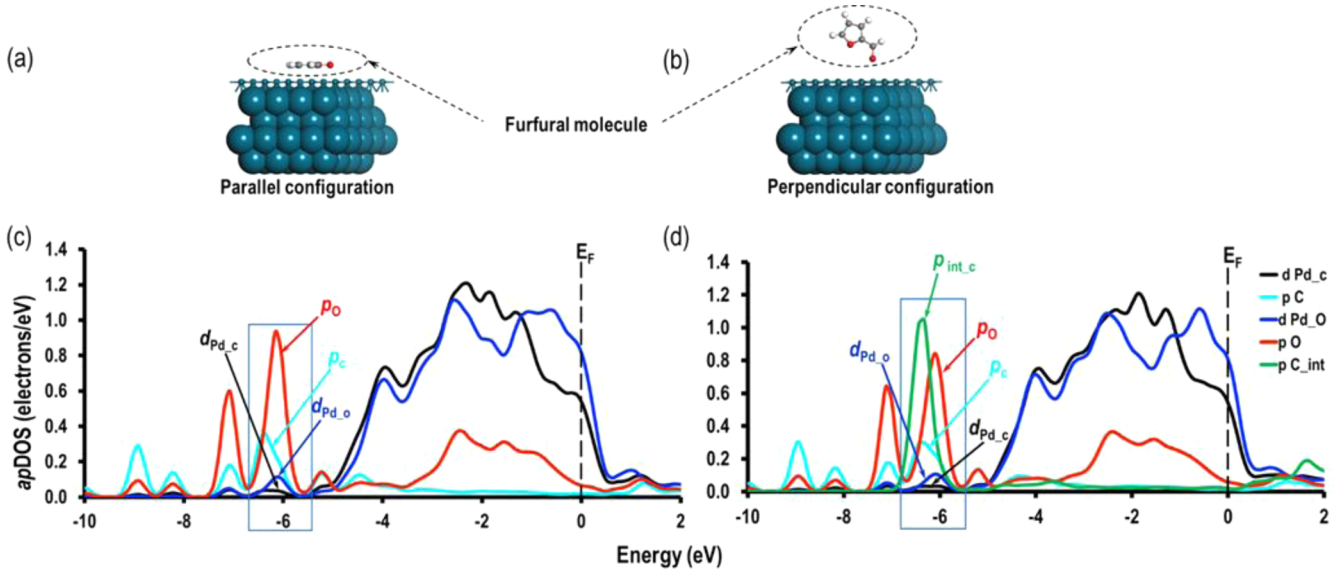

Figure 8. (a) Parallel and (b) perpendicular configurations of furfural on the Pd(111) surface. (c) *ap*DOS for pristine Pd(111) and (d) *ap*DOS for furfural on the PdC(111) surface. Black and blue lines represent the signatures for Pd d orbitals close to C and O atoms, respectively. Red, aqua, and green lines represent the p orbitals due to C, O, and interstitial C atoms, respectively.

which is slightly more negative than the previously reported value of −1.830 eV, which can be accounted for by the different versions of DFT-D approaches used.[21] The adsorption energies for Pd_{top}, Pd_{bridge}, and Pd_{hollow} configurations are −0.632, −0.940, and −2.185 eV, respectively, with relaxed structures of Pd_{top} and Pd_{bridge} retaining a perpendicular orientation. However, it is interesting to note that for the Pd_{hollow} site the furfural molecule attained a parallel configuration to the surface after relaxation ($Pd_{hollow\text{-}parallel}$) and is comparable in energy to the $Pd_{parallel}$ configuration. The adsorption energies obtained confirm that the parallel configuration of furfural binding is more stable than the perpendicular orientation. Subsequently, we investigated the increase in Pd−Pd bond distances, as a result of carbidization, in bulk Pd (by 0.095 Å) and subsurface of Pd(111) (by 0.057 Å) (Figures S10 and S11 in the Supporting Information), which were consistent with experimentally determined values of partially carbidized Pd nanoparticles.[43,44] We found that the increase in Pd−Pd distance correlated with an increased adsorption energy for furfural. The calculated adsorption energy for this system is −1.613 eV, confirming that adsorption of furfural is more favorable on pristine Pd(111), in comparison to PdC(111). Furthermore, on comparing the geometry of furfural on pristine and carbide systems we find that in both cases parallel adsorption is preferred, although there are some minor differences in the planarity of the furfural adsorption (Table S7 in the Supporting Information).

To assess this change in stability, we analyzed the atom projected partial density of states (*ap*PDOS) of the C and O atoms of the furfural molecule and Pd atoms of the Pd(111) and PdC(111) surfaces closest to each other. For convenience, the Fermi energy (E_F) is shifted to 0, which is represented by a dotted line in Figure 8c,d. From the analysis of *ap*PDOS we see that around −7.0 to −5.5 eV (Figure 8c,d) there is a strong interaction between the p orbitals, of C and O atoms of furfural, with the d orbital signatures of Pd atoms on the Pd(111) surface. However, on incorporation of an interstitial C atom, another sharp signature due to the C p orbital appears around this region, which has a higher contribution than the p-orbital signatures due to C and O atoms of the furfural molecule. The interaction of the C p signatures, due to interstitial C atoms, interact more strongly with the nearby Pd atoms and result in a weakening of the interaction of furfural C and O atoms with the Pd(111) surface. As a consequence, adsorption of furfural is more favored on pristine Pd(111), in comparison to PdC(111).

CONCLUSIONS

We have demonstrated the tandem optimization of the colloidal preparation of Pd nanoparticles, through adapting a simple and systematic combination of choice of solvent and temperature of reduction. These parameters allow us to tune both the size domains of Pd nanoparticles and available reaction sites, which directs the performance toward the hydrogenation of furfural. Reduced Pd NP size was achieved by lowering the temperature of colloidal reduction. For the catalyst prepared at 1 °C in water the average particle size was found to be 2.5 nm; however, we were also able to detect clusters of Pd with <20 atoms. For the B series prepared at −30 °C, an average particle size of 1.4 nm was produced, which is smaller than has been previously reported for Pd NPs prepared through a PVA/$NaBH_4$ colloidal route. Site-selective catalysis was enabled by adjusting the solvent of colloid preparation; the Pd/TiO_2 catalysts prepared using a water−ethanol solvent were found to have a larger proportion of available corner and edge sites, which were able to direct the selectivity of the furfural hydrogenation products. We propose that the greater number of available corner and edge sites adsorb furfural perpendicular to the nanoparticle surface, resulting in greater selectivity to form furfuryl alcohol over the complete reduction product, tetrahydrofurfuryl alcohol. We also find that the selectivity profile does not correspond solely to particle size; for the B series furfuryl alcohol selectivity decreases with increasing particle size, whereas for the A series the inverse relationship is found. The available sites are therefore not just a result of particle size but are also a consequence of the interaction of the protecting agent with the NPs prepared. This influence was also manifested in recycling studies, where those catalysts prepared in water−ethanol were more robust than those prepared solely

DOI: 10.1021/acscatal.6b03190
ACS Catal. 2017, 7, 2266−2274

in water. By assessing the EXAFS of the used catalysts, we were able to identify a Pd−Pd lattice expansion. This is attributed to the formation of Pd carbide, which we propose is responsible for the deactivation observed. This assertion is supported by computational modeling studies, which show that the carbidization of Pd reduces the binding energy of furfural, leading to a lowering of catalytic activity. To our knowledge this is the first report of this proposed deactivation pathway for the hydrogenation of α,β-unsaturated aldehydes.

■ ASSOCIATED CONTENT

Supporting Information

The Supporting Information is available free of charge on the ACS Publications website at DOI: 10.1021/acscatal.6b03190.

TEM HAADF images with supporting Pd particle size distribution histograms, EXAFS fitting parameters, CO-chemisorption IR spectra, microwave plasma-atomic emission spectroscopy, computational studies, and additional catalytic data for furfural hydrogenation can be found in the Supporting Information. The original data presented in this manuscript can be accessed at http://doi.org/10.5258/SOTON/405197 (PDF)

■ AUTHOR INFORMATION

Corresponding Authors

*E-mail for A.V.: alberto.villa@unimi.it.
*E-mail for P.P.W.: p.p.wells@soton.ac.uk.

ORCID

Nan Jian: 0000-0003-2179-8237
Peter P. Wells: 0000-0002-0859-9172

Author Contributions

S.M.R. synthesized catalysts, performed catalyst characterization (TEM, IR, and XAFS), and had major contributions to the writing of the manuscript. M.P. helped to synthesize the catalysts and performed TEM. A.V. and C.E.C.-T. conducted all of the liquid phase hydrogenation experiments. N.J. and R.E.P. conducted HAADF STEM. A.C., C.R.A.C., and A.T. performed all of the computational studies. N.D and C.R.A.C. were involved in project discussions and supervised the project. P.P.W. and A.V. had major contributions to the writing of the manuscript, were involved in all of the project discussions, and supervised the project. All authors discussed the results and commented on the manuscript.

Notes

The authors declare no competing financial interest.

■ ACKNOWLEDGMENTS

The UK Catalysis Hub Consortium is funded by the EPSRC (portfolio grants EP I019693, EP/K014706/1, EP/K014668/1, EP/K014854/1 and EP/K014714/1). Via our membership in the UKs HEC Materials Chemistry Consortium, which is funded by the EPSRC (EP/L000202), this work used the ARCHER UK National Supercomputing Service. The authors wish to acknowledge the Diamond Light Source for provision of beamtime (SP10306). Diamond Light Source is also thanked for the outstanding support of the staff on B18: Prof. Andrew Dent, Dr. Giannantonio Cibin, Dr. Diego Gianolio, Dr. Stephen Parry, and Mr. Phil Robbins. The RCaH is acknowledged for use of facilities and support of their staff. Kristina Penman is thanked for performing the MP-AES measurements. UK Catalysis Hub is kindly thanked for resources and support provided via our membership of the UK Catalysis Hub Consortium.

■ REFERENCES

(1) Hu, X.; Westerhof, R. J. M.; Dong, D.; Wu, L.; Li, C. Z. *ACS Sustainable Chem. Eng.* **2014**, *2*, 2562−2575.
(2) Lange, J. P.; Van der Heide, E.; Van Buijtenen, J.; Price, R. *ChemSusChem* **2012**, *5*, 150−166.
(3) Huber, G. W.; Iborra, S.; Corma, A. *Chem. Rev.* **2006**, *106*, 4044−4098.
(4) Li, G.; Li, N.; Li, S.; Wang, A.; Cong, Y.; Wang, X.; Zhang, T. *Chem. Commun.* **2013**, *49*, 5727−5729.
(5) Corma, A.; Iborra, S.; Velty, A. *Chem. Rev.* **2007**, *107*, 2411−2502.
(6) Yan, K.; Wu, S.; Lafleur, T.; Jarvis, C. *Renewable Sustainable Energy Rev.* **2014**, *38*, 663−676.
(7) Nakagawa, Y.; Nakazawa, H.; Watanabe, H.; Tomishige, K. *ChemCatChem* **2012**, *4*, 1791−1797.
(8) Panagiotopoulou, P.; Vlachos, D. G. *Appl. Catal., A* **2014**, *480*, 17−24.
(9) Nakagawa, Y.; Takada, K.; Tamura, M.; Tomishige, K. *ACS Catal.* **2014**, *4*, 2718−2726.
(10) Biradar, N. S.; Hengne, A. M.; Birajdar, S. N.; Niphadkar, P. S.; Joshi, P. N.; Rode, C. V. *ACS Sustainable Chem. Eng.* **2014**, *2*, 272−281.
(11) Rao, R.; Dandekar, A.; Baker, R. T. K.; Vannice, M. A. *J. Catal.* **1997**, *171*, 406−419.
(12) Nagaraja, B. M.; Padmasri, A. H.; Raju, B. D.; Rao, K. S. R. *J. Mol. Catal. A: Chem.* **2007**, *265*, 90−97.
(13) Rao, R. S.; Baker, R. T. K.; Vannice, M. A. *Catal. Lett.* **1999**, *60*, 51−57.
(14) Sitthisa, S.; Resasco, D. E. *Catal. Lett.* **2011**, *141*, 784−791.
(15) Sitthisa, S.; Sooknoi, T.; Ma, Y.; Balbuena, P. B.; Resasco, D. E. *J. Catal.* **2011**, *277*, 1−13.
(16) Sitthisa, S.; An, W.; Resasco, D. E. *J. Catal.* **2011**, *284*, 90−101.
(17) Aldosari, O. F.; Iqbal, S.; Miedziak, P. J.; Brett, J. L.; Jones, D. R.; Liu, X.; Edwards, J. K.; Morgan, D. J.; Knight, D. K.; Hutchings, G. *Catal. Sci. Technol.* **2016**, *6*, 234−242.
(18) Iqbal, S.; Liu, X.; Aldosari, O. F.; Miedziak, P. J.; Edwards, J. K.; Brett, J. L.; Akram, A.; King, G. M.; Davies, T. E.; Morgan, D. J.; Knight, D. K.; Hutchings, G. *Catal. Sci. Technol.* **2014**, *4*, 2280−2286.
(19) King, G. M.; Iqbal, S.; Miedziak, P. J.; Brett, J. L.; Kondrat, S. A.; Yeo, B. R.; Liu, X.; Edwards, J. K.; Morgan, D. J.; Knight, D. K.; Hutchings, G. J. *ChemCatChem* **2015**, *7*, 2122−2129.
(20) Shekhar, R.; Barteau, M. A.; Plank, R. V.; Vohs, J. M. *J. Phys. Chem. B* **1997**, *101*, 7939−7951.
(21) Vorotnikov, V.; Mpourmpakis, G.; Vlachos, D. G. *ACS Catal.* **2012**, *2*, 2496−2504.
(22) Bhogeswararao, S.; Srinivas, D. *J. Catal.* **2015**, *327*, 65−77.
(23) Schoenbaum, C. A.; Schwartz, D. K.; Medlin, J. W. *Acc. Chem. Res.* **2014**, *47*, 1438−1445.
(24) Pang, S. H.; Schoenbaum, C. A.; Schwartz, D. K.; Medlin, J. W. *Nat. Commun.* **2013**, *4*, 2448.
(25) Pang, S. H.; Schoenbaum, C. A.; Schwartz, D. K.; Medlin, J. W. *ACS Catal.* **2014**, *4*, 3123−3131.
(26) Rogers, S. M.; Catlow, C. R. A.; Chan-Thaw, C. E.; Gianolio, D.; Gibson, E. K.; Gould, A. L.; Jian, N.; Logsdail, A. J.; Palmer, R. E.; Prati, L.; Dimitratos, N.; Villa, A.; Wells, P. P. *ACS Catal.* **2015**, *5*, 4377−4384.
(27) Wang, Z. W.; Toikkanen, O.; Yin, F.; Li, Z. Y.; Quinn, B. M.; Palmer, R. E. *J. Am. Chem. Soc.* **2010**, *132*, 2854.
(28) Jian, N.; Palmer, R. E. *J. Phys. Chem. C* **2015**, *119*, 11114−11119.
(29) Ravel, B.; Newville, M. *J. Synchrotron Radiat.* **2005**, *12*, 537−541.
(30) Newville, M. *J. Synchrotron Radiat.* **2001**, *8*, 322−324.
(31) Grimme, S. *J. Comput. Chem.* **2006**, *27*, 1787−1799.
(32) Blöchl, P. E. *Phys. Rev. B: Condens. Matter Mater. Phys.* **1994**, *50*, 17953−17979.

DOI: 10.1021/acscatal.6b03190
ACS Catal. 2017, 7, 2266−2274

(33) Kresse, G.; Hafner. *Phys. Rev. B: Condens. Matter Mater. Phys.* **1994**, *49*, 14251−14269.
(34) Kresse, G.; Hafner. *Phys. Rev. B: Condens. Matter Mater. Phys.* **1993**, *47*, 558−561.
(35) Kresse, G.; Furthmüller. *Phys. Rev. B: Condens. Matter Mater. Phys.* **1996**, *54*, 11169−11186.
(36) Perdew, J. P.; Burke, K.; Ernzerhof, M. *Phys. Rev. Lett.* **1996**, *77*, 3865−3868.
(37) Singh-Miller, N. E.; Marzari, N. *Phys. Rev. B: Condens. Matter Mater. Phys.* **2009**, *80*, 235407.
(38) Su, R.; Tiruvalam, R.; He, Q.; Dimitratos, N.; Kesavan, L.; Hammond, C.; Lopez-Sanchez, J. A.; Bechstein, R.; Kiely, C. J.; Hutchings, G. J.; Besenbacher, F. *ACS Nano* **2012**, *6*, 6284−6292.
(39) Wells, P. P.; Crabb, E. M.; King, C. R.; Wiltshire, R.; Billsborrow, B.; Thompsett, D.; Russell, A. E. *Phys. Chem. Chem. Phys.* **2009**, *11*, 5773−5781.
(40) Lear, T.; Marshall, R.; Lopez-Sanchez, J. A.; Jackson, S. D.; Klapotke, T. M.; Baumer, M.; Rupprechter, G.; Freund, H. J.; Lennon, D. *J. Chem. Phys.* **2005**, *123*, 174706.
(41) Hadjiivanov, K. I.; Vayssilov, G. N. *Adv. Catal.* **2002**, *47*, 307−511.
(42) Zhu, H. Q.; Qin, Z. F.; Shan, W. J.; Shen, W. J.; Wang, J. G. *J. Catal.* **2004**, *225*, 267−277.
(43) Tew, M. W.; Nachtegaal, M.; Janousch, M.; Huthwelker, T.; Van Bokhoven, J. A. *Phys. Chem. Chem. Phys.* **2012**, *14*, 5761−5768.
(44) McCaulley, J. A. *J. Phys. Chem.* **1993**, *97*, 10372−10379.
(45) Bugaev, A. L.; Guda, A. A.; Lazzarini, A.; Lomachenko, K. A.; Groppo, E.; Pellegrini, R.; Piovano, A.; Emerich, H.; Soldatov, A. V.; Bugaev, L. A.; Dmitriev, V. P.; Van Bokhoven, J. A.; Lamberti, C. *Catal. Today* **2017**, *283*, 119−126.
(46) McCaulley, J. A. *Phys. Rev. B: Condens. Matter Mater. Phys.* **1993**, *47*, 4873−4879.
(47) Yang, B.; Burch, R.; Hardacre, C.; Headdock, G.; Hu, P. *J. Catal.* **2013**, *305*, 264−276.
(48) Yang, B.; Burch, R.; Hardacre, C.; Hu, P.; Hughes, P. *Surf. Sci.* **2016**, *646*, 45−49.

DOI: 10.1021/acscatal.6b03190
ACS Catal. 2017, 7, 2266−2274